Rock Mechanics and Rock Engineering
https://doi.org/10.1007/s00603-022-02899-4

TECHNICAL NOTE

Stability of Spherical Cavity in Hoek–Brown Rock Mass

Suraparb Keawsawasvong[1] · **Jim Shiau**[2]

Received: 7 December 2021 / Accepted: 17 April 2022

Highlights

- A state of art approach to evaluate the stability of Hoek–Brown rock mass with a spherical cavity.
- Rigorous upper bound and lower bound solutions of stability factors are solved using advanced finite element limit analysis.
- Comprehensive design charts, tables and equations are presented for stability evaluation.

Keywords Rock mass · Hoek–Brown · Finite element limit analysis · Stability criterion

1 Introduction

A karst cavity is a type of underground cavities in rock masses that can be formed from the dissolution of soluble rocks such as limestone, dolomite, and gypsum (Huang et al. 2017). Collapse of a karst cavity is a serious threat to human lives as well as an economic or environmental disaster. Therefore, obtaining information about karst cavity sizes and locations as well as the stability assessment of a spherical opening is of paramount importance to assure the safety of the existence of underground cavities.

The failure patterns of underground cavities in soils were investigated by Craig (1990) and Abdulla (1995) using centrifuge model tests as well as numerical and analytical techniques (e.g., Drumm et al. 1990; Abdulla and Goodings 1996; Tharp 1999; Vaziri et al. 2001; Augarde et al. 2003; Keawsawasvong and Ukritchon 2019; Shiau and Al-Asadi 2020; Shiau et al. 2021; Keawsawasvong 2021). The finite element limit analysis (FELA) is a powerful numerical technique that has been widely used by many researchers to determine the upper bound (UB) or the lower bound (LB) solutions of plastic collapse load of various stability problems based on the plastic bound theorems (Sloan 2013; Drucker et al. 1952). By using FELA, exact collapse loads can be accurately bracketed from UB and LB solutions. For the stability analysis of underground cavities, several researchers employed FELA to numerically solve the solutions to this problem (Augarde et al. 2003; Shiau and Smith 2006, Keawsawasvong and Ukritchon 2019; Shiau et al. 2016a, b; Keawsawasvong 2021). However, their solutions are limited to the cases of underground cavities in soils obeying the Mohr–Coulomb failure criterion. It is well known that rock masses are discontinuous materials with joints and fractures. The curved shape of the true failure envelope of rock masses cannot be replaced by a linear expression of the Mohr–Coulomb failure criterion. Consequently, it is seldom used to predict the stability of underground cavities in rock masses, in spite that the Mohr–Coulomb failure criterion constitutes a good approximation of the true failure envelope for some weak rock masses (Hoek et al. 2002).

The Hoek–Brown (HB) failure criterion (Hoek et al. 2002) has been widely accepted and adopted by many geotechnical engineers to predict the failure of intact rocks. It is an empirical failure criterion and the basic idea of the Hoek–Brown criterion was to start with the properties of intact rock, and then the factors to reduce those properties

✉ Jim Shiau
jim.shiau@usq.edu.au

Suraparb Keawsawasvong
ksurapar@engr.tu.ac.th

[1] Department of Civil Engineering, Thammasat School of Engineering, Thammasat University, Pathumthani 12120, Thailand

[2] School of Civil Engineering and Surveying, University of Southern Queensland, Toowoomba, QLD 4350, Australia

Published online: 09 May 2022

are added to the equation because of the existence of joints in the rock (Hoek et al. 2002). By adopting the HB failure criterion into FELA, many researchers have investigated the stability of tunnels and underground openings in HB rock masses under plane strain conditions (e.g., Fraldi and Guarracino 2009; Ukritchon and Keawsawasvong 2019a, b; Keawsawasvong and Ukritchon 2020; Rahaman and Kumar 2020; Xiao et al. 2018, 2019, 2021; Wu et al. 2020; Zhang et al. 2019).

Currently, there is no solution or stability criterion published for stability assessment of cavities in HB rock masses under axisymmetric conditions in the literature. This technical note aims to develop and propose a stability criterion for stability assessment of cavities in HB rock masses based on UB and LB solutions obtained from axisymmetric FELA. The considered parameters include the cover-depth ratio of cavities and the HB material parameters that have significant influences on the normalized collapse pressure applied at the rock surface above a cavity. Nonlinear regression analysis is employed to develop a closed-form approximate equation of this problem. This developed equation is valuable for engineers in practice to estimate the stability of underground cavities in rock masses.

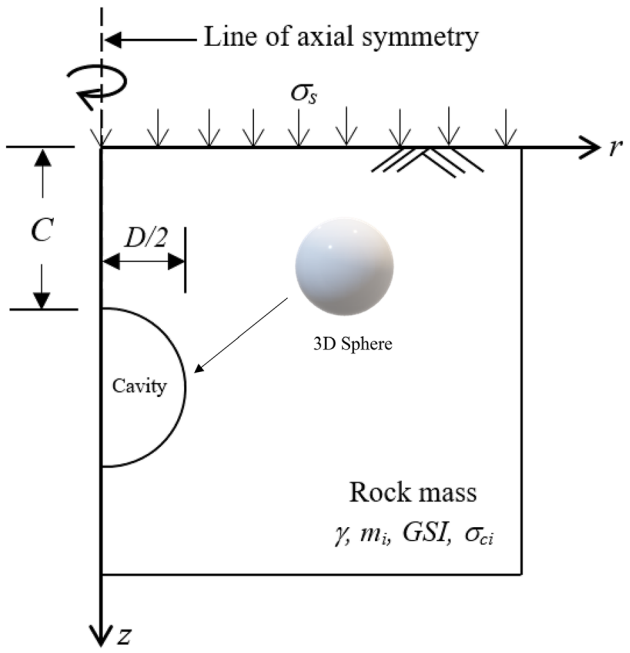

Fig. 1 The stability problem under axisymmetry

2 Problem Statement and FELA Modelling

Figure 1 shows the problem definition of a spherical cavity in a rock mass. The cavity has a diameter (D) and a cover depth (C). A uniform surcharge (σ_s) at the collapse is applied over the surface area. The stability problem is investigated under 2D axisymmetric conditions. The work stated herein used the Hoek–Brown (HB) failure criterion (Hoek et al. 2002) to investigate the failure of a cavity in a rock mass. The Hoek–Brown (HB) parameters for a rock mass include σ_{ci}, GSI, and m_i, and a unit weight of γ.

The expression of the HB failure criterion is in the form of a power-law relationship between the effective major and minor principal stresses (σ_1 and σ_3) as shown in Eq. (1).

$$-\sigma_3 = -\sigma_1 + \sigma_{ci}\left(-m_b\frac{\sigma_1}{\sigma_{ci}} + s\right)^{\alpha} \tag{1}$$

It is to be noted that the compression negative sign convention applies to Eq. 1 and σ_{ci} denotes the uniaxial compressive strength of intact rock masses. Other parameters such as m_b, s, and α are expressed in Eqs. (2)–(4).

$$m_b = m_i \exp\left(\frac{GSI - 100}{28 - 14DF}\right) \tag{2}$$

$$s = \exp\left(\frac{\mathrm{GSI} - 100}{9 - 3\mathrm{DF}}\right) \tag{3}$$

$$\alpha = \frac{1}{2} + \frac{1}{6}\left(e^{-\frac{\mathrm{GSI}}{15}} - e^{-\frac{20}{3}}\right) \tag{4}$$

In the HB failure criterion, GSI is the geological strength index describing the quality of an in-situ rock mass. A GSI of 10 represents an extremely poor rock mass whilst 100 is used for intact rock. m_i is the parameter used to describe the frictional strength of the intact rock mass. Noting that DF is the disturbance factor that has the range of 0–1, an undisturbed in-situ rock mass with DF = 0 is studied throughout the paper.

Using the concept of dimensionless ratios for practical design purposes, the stability solutions are determined through the use of five dimensionless variables as shown in Eq. (5).

$$\frac{\sigma_s}{\sigma_{ci}} = f\left(\frac{C}{D}, \frac{\sigma_{ci}}{\gamma D}, m_i, \mathrm{GSI}\right) \tag{5}$$

where σ_s/σ_{ci} is the normalized collapse surcharge; C/D is the cover depth ratio; $\sigma_{ci}/\gamma D$ *is* the normalized uniaxial compressive strength.

The computer program OptumG2 (FELA, OptumCE 2019) is employed to perform the numerical analyses of the upper bound (UB) and lower bound (LB) finite element limit analysis (FELA). The FELA is based on the plastic bound theorems for a perfectly plastic material with an associated flow rule in conjunction with the finite element discretization and the mathematical optimization (Sloan 2013). The results from FELA include the UB and LB solutions that can bracket the true limit load from above and below.

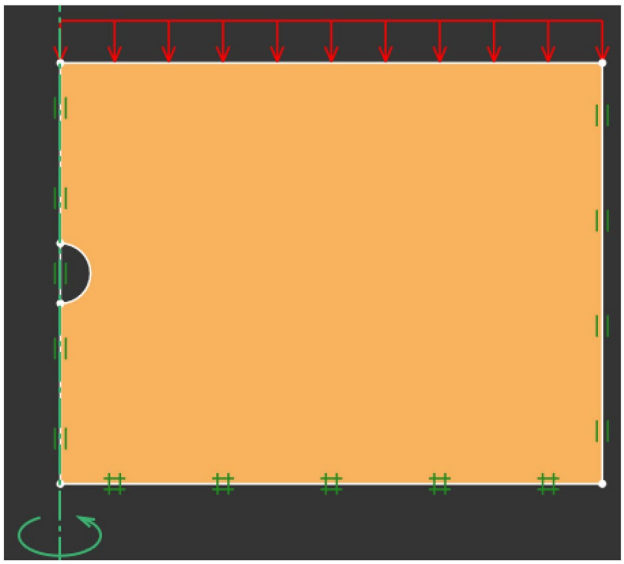

Fig. 2 A spherical cavity under axisymmetry

In UB FELA, the rock mass is discretized by using six-noded quadratic triangular elements to describe the overall velocity fields. In LB FELA, the rock mass is modelled using three-noded triangular elements to describe the linear stress field. The UB and LB solutions of this problem are computed by solving the optimization problem that minimizes (for the UB method) or maximizes (for LB method) the active surface pressure (σ_s) i.e., the collapse pressure at the ground surface. The mesh adaptivity technique (e.g., Ciria et al. 2008) is a powerful feature for improving LB and UB solutions. By activating this feature, more elements are added to the sensitive regions with large shear strain gradients at any iteration step, aiming to bridge the differences between UB and LB solutions. Five iterations of mesh adaptivity were used for all UB and LB simulations in the study, with 5000–10,000 elements in all analyses. It is interesting to note that the current technique reveals the location of a possible failure mechanism at the final stage of mesh adaptivity.

Figure 2 shows a typical domain for the analysis of a spherical cavity. The left boundary is the plane of axisymmetry where only vertical movements can take place. The same condition applies to the right boundary. Nevertheless, velocities are fixed in both vertical and horizontal directions at the bottom boundary. At the rock surface, there is a uniform surcharge σ_s applied over the surface area. The size of the domain is chosen to be large enough to avoid any interferences due to boundary effects. The current model does not allow internal pressure inside the cavity.

Table 1 Selected numerical results of σ_s/σ_{ci} for cavities in rock masses

$\sigma_{ci}/\gamma D$	*GSI*	m_i	*C/D*	σ_s/σ_{ci} (LB)	σ_s/σ_{ci} (UB)	σ_s/σ_{ci} (Avg)	%Diff
100	40	5	1	0.848	0.882	0.865	3.98
100	40	5	5	3.827	4.007	3.917	4.60
100	40	30	1	5.429	5.567	5.498	2.51
100	40	30	5	23.920	24.225	24.073	1.27
100	100	5	1	9.450	9.769	9.610	3.32
100	100	5	5	36.250	37.140	36.695	2.43
100	100	30	1	46.850	46.330	46.590	1.12
100	100	30	5	193.200	196.320	194.760	1.60
1000	40	5	1	0.869	0.897	0.883	3.18
1000	40	5	5	3.898	3.920	3.909	0.56
1000	40	30	1	5.174	5.413	5.294	4.51
1000	40	30	5	23.990	24.288	24.139	1.23
1000	100	5	1	9.506	9.818	9.662	3.23
1000	100	5	5	37.110	37.549	37.330	1.18
1000	100	30	1	44.780	46.410	45.595	3.57

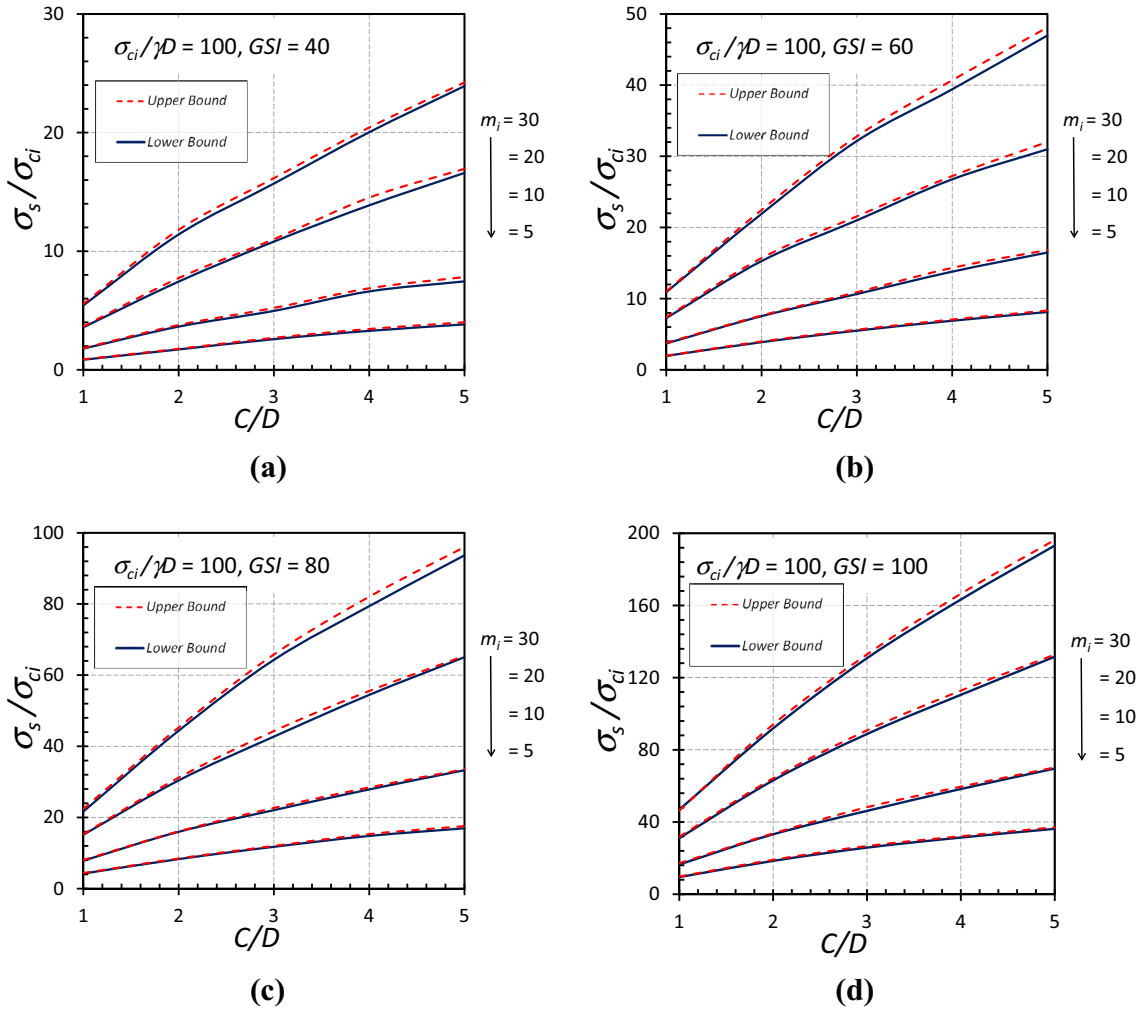

Fig. 3 Effect of *C/D* on the normalized collapse pressure σ_s/σ_{ci} **a** GSI = 40, **b** GSI = 60, **c** GSI = 80 and **d** GSI = 100

3 Results and Discussions

The chosen ranges of dimensionless parameters for the study are for $\sigma_{ci}/\gamma D = 100$–$\infty$, $GSI = 40 - 100$, $m_i = 5$–30 and $C/D = 1$–5. A total of 320 computed LB and UB solutions are obtained. Table 1 summarizes sixteen examples of computed LB and UB solutions of the normalized collapse surcharge σ_s/σ_{ci}. The differences between UB and LB solutions with respect to their averages for all cases are also reported. These results show that the rigorous UB and LB results can bracket the "exact" solution to within 5% for all cases. Other numerical results are not shown here for the sake of limited space. They are available upon request. Graphically, selected LB and UB solutions of σ_s/σ_{ci} are presented in Figs. 3, 4, 5, and 6 for demonstrating the effects of *C/D*, *GSI*, m_i, and $\sigma_{ci}/\gamma D$ respectively.

Figure 3a–d show that σ_s/σ_{ci} increases as the cover depth *C/D* increases. This trend is for $\sigma_{ci}/\gamma D = 100$ and all *GSI* values presented. In general, the larger the value of m_i is, the greater the increase rate. The effect of *GSI* on σ_s/σ_{ci} is shown in Fig. 4, where $\sigma_{ci}/\gamma D = 100$ and $m_i = 5$, 10, 20, and 30. The figure shows a nonlinear relationship between *GSI* and σ_s/σ_{ci}. An increase in *GSI* results in an exponential increase in $\sigma_s/_{ci}$, as reflected in the mathematic equations of HB failure criterion in Eqs. (2)–(4).

The effect of m_i on σ_s/σ_{ci} is illustrated in Fig. 5a–d for four different values of GSI = 40, 60, 80, and 100. The study is for $\sigma_{ci}/\gamma D = \infty$ and five cover depth ratios $C/D = 1$–5. In general, σ_s/σ_{ci} increases linearly as m_i

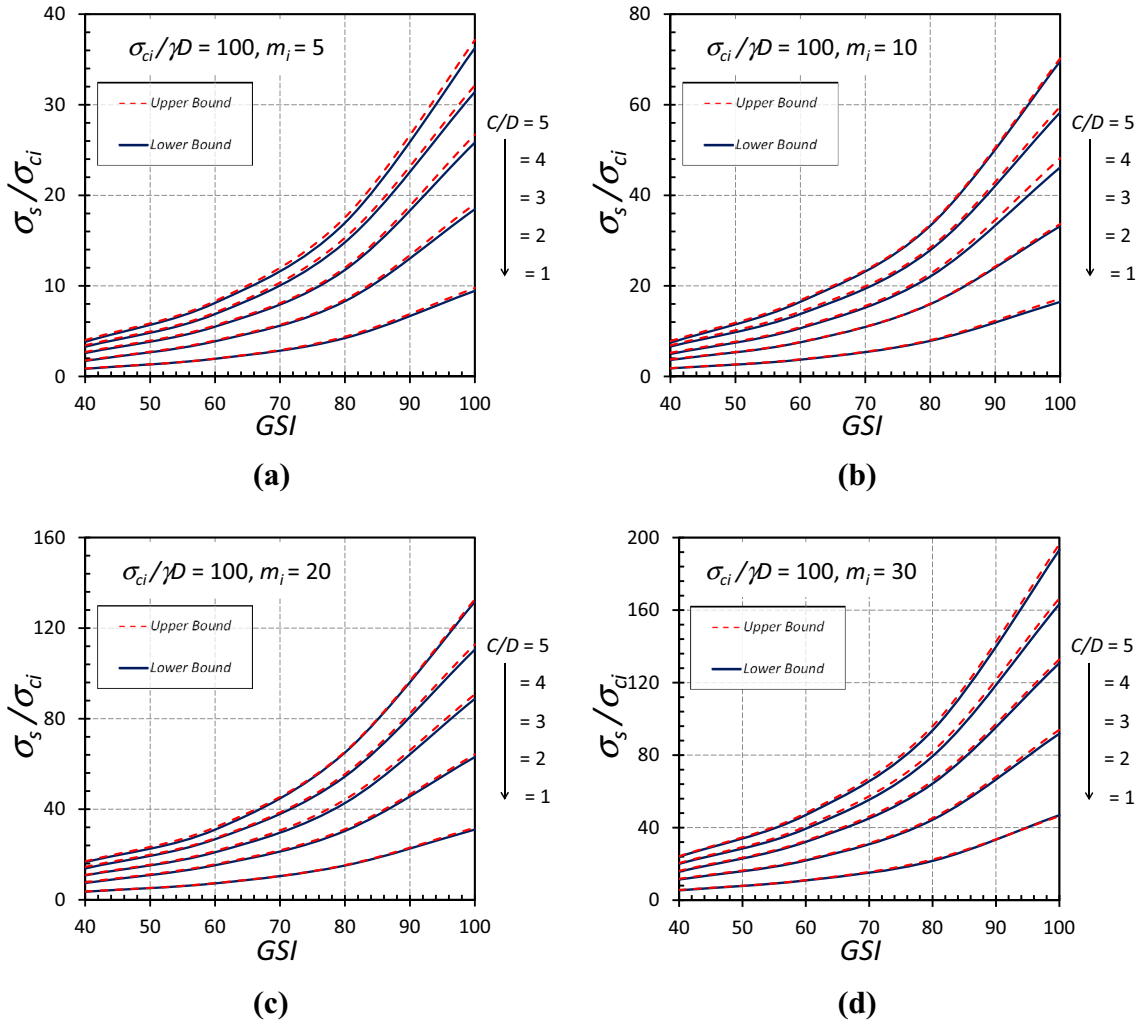

Fig. 4 Effect of *GSI* on the normalized collapse pressure σ_s/σ_{ci} **a** $m_i=5$, **b** $m_i=10$, **c** $m_i=20$ and **d** $m_i=30$

increases for all *C/D*. Note that as *C/D* increases, the gradient of the linear line also increases. Figure 6 shows the effect of $\sigma_{ci}/\gamma D$ on σ_s/σ_{ci}. This is for the cases of $m_i=20$. It is clear that the effect $\sigma_{ci}/\gamma D$ on σ_s/σ_{ci} is insignificant for all *C/D*, given all the horizontal lines in the figure. Although it is physically impossible to have a weightless rock, the obtained results in Figs. 5 and 6 for $\sigma_{ci}/\gamma D=\infty$ are simply representatives of a very "strong" rock (i.e., very large strength ratio). Numerically, we can either put a very large value of σ_{ci} or a very small γ to achieve the numerical results, which are needed to develop the stability criterion in the next section.

Figure 7 presents upper bound adaptive meshes of four various cover depth ratios *C/D*. The chosen rock mass is for GSI = 80, $m_i=10$, and $\sigma_{ci}/\gamma D=100$. It is important to note that the automatic adaptive meshing technique utilizes shear power dissipation as the control variable for re-meshing estimation. The number of elements in areas with very high shear power dissipation is automatically increased through successive iterations using the adaptive technique. Although the final adaptive mesh so produced resembles a so-called failure mechanism, it is common to use the contour plots of shear power dissipation to depict possible failure mechanisms of a soil structure, as it provides a good indicator of the intensity of non-zero plastic strains. Technically speaking, the actual values of the contour are not important in a perfectly plastic material model using FELA, and therefore the contour bars for

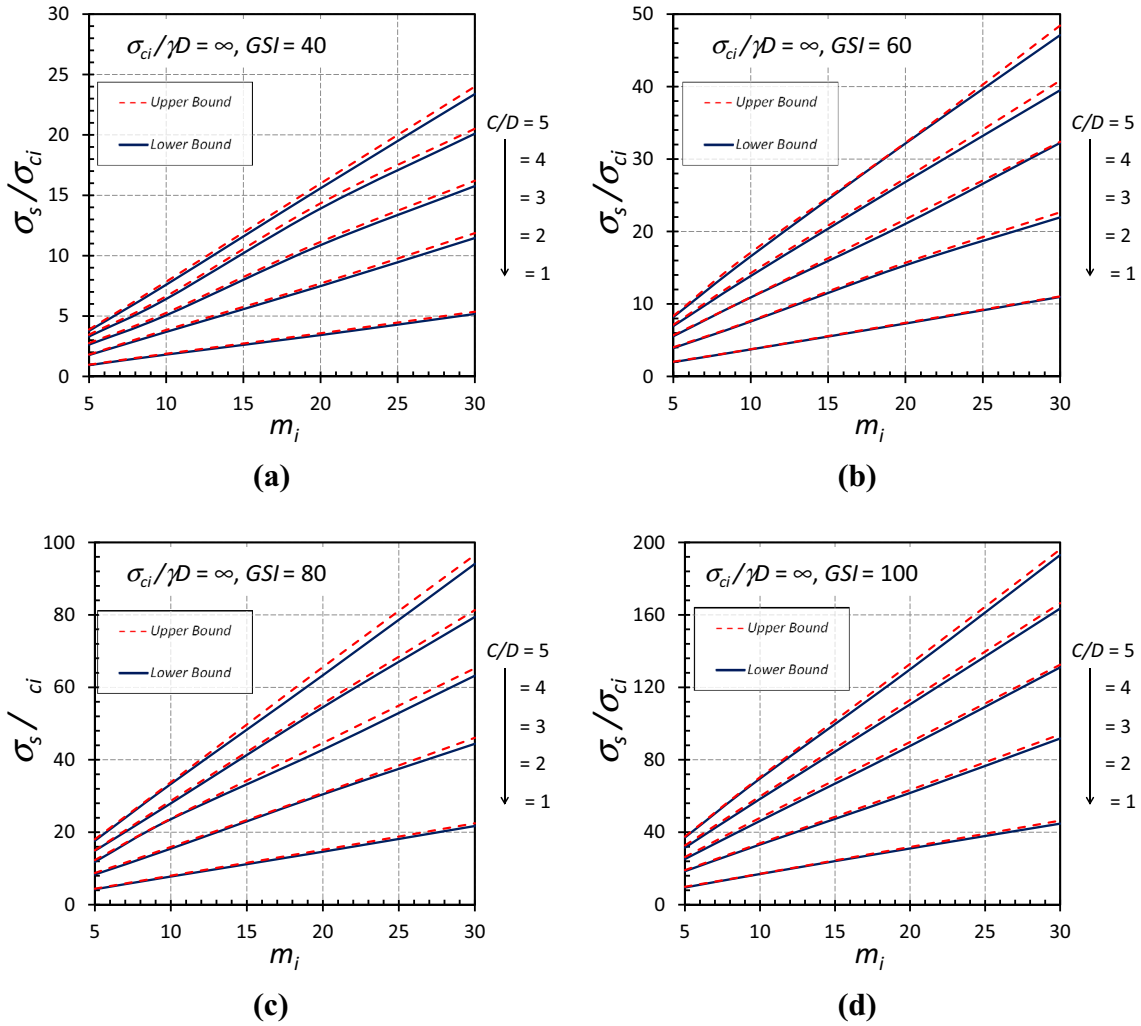

Fig. 5 Effect of m_i on the normalized collapse pressure σ_s/σ_{ci} **a** GSI = 40, **b** GSI = 60, **c** GSI = 80 and **d** GSI = 100

these plots are not normally shown in technical documents. Figure 8 demonstrates such a contour plot obtained from the kinematic solutions (or UB solutions). Both Figs. 7 and 8 have shown that the larger the cover depth ratio *C/D*, the larger the size of the plastic shear zone, and the greater the rock stability (σ_s/σ_{ci}). For $C/D = 5$, the failure zone appears to initiate from the invert, whilst for $C/D = 1$, a more chimney type of vertical slippage is observed. The information on surface failure extent may be useful in decision making in relation to the development of evacuation zone.

4 Stability Criterion

Design tables and charts of σ_s/σ_{ci} have been presented in the earlier sections. Nevertheless, in most cases, the limit pressure σ_s is greater than the unconfined compressive strength of the intact rock σ_{ci}. To obtain solutions with small values of σ_s/σ_{ci}, an approximate expression for calculating collapse pressures at the rock surface above a cavity is developed by using a curve fitting method. The average values of UB and LB are employed to determine an appropriate mathematical expression. The proposed stability criterion is presented in Eq. (6).

$$\sigma_s = N_c \sigma_{ci} - N_\gamma \gamma D \tag{6}$$

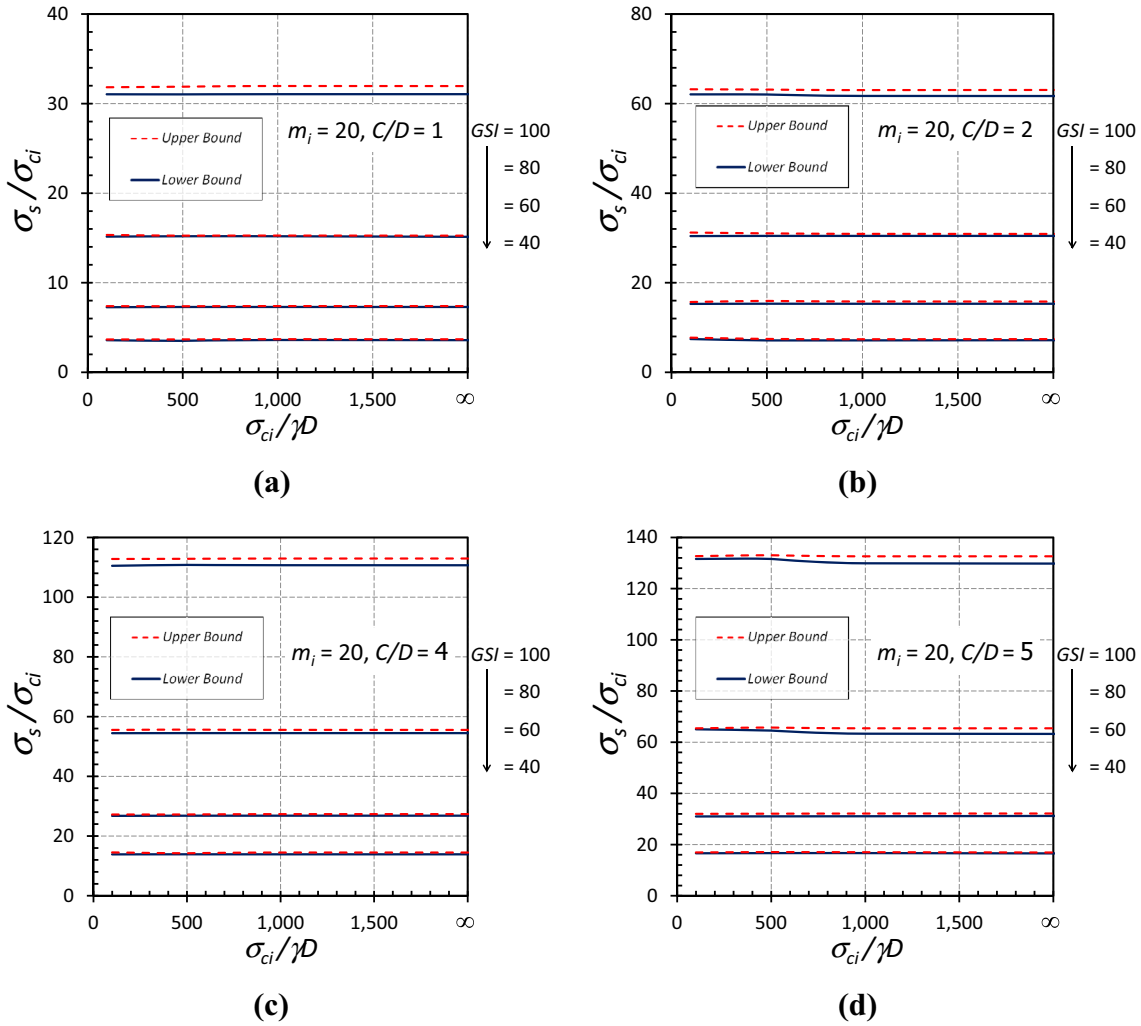

Fig. 6 Effect of $\sigma_{ci}/\gamma D$ on the normalized collapse pressure σ_s/σ_{ci} **a** $C/D=1$, **b** $C/D=2$, **c** $C/D=4$ and **d** $C/D=5$

Both N_c and N_γ are to be determined using Eqs. (7)–(11) with known values of C/D, GSI, m_i, and $\sigma_{ci}/\gamma D$

$$N_c = F_1 + F_2 m_i \tag{7}$$

$$N_\gamma = F_3 \tag{8}$$

$$F_1 = \mathrm{GSI}\left[b_1 + b_2\frac{C}{D} + b_3\left(\frac{C}{D}\right)^2\right] + \mathrm{GSI}^2\left[c_1 + c_2\frac{C}{D} + c_3\left(\frac{C}{D}\right)^2\right] \tag{9}$$

$$F_2 = e_1 + e_2\frac{C}{D} + \mathrm{GSI}\left[f_1 + f_2\frac{C}{D} + f_3\left(\frac{C}{D}\right)^2\right] + \mathrm{GSI}^2\left[g_1 + g_2\frac{C}{D}\right] + \mathrm{GSI}^3\left(d_2\frac{C}{D}\right) \tag{10}$$

$$F_3 = -a_1 - a_2\frac{C}{D} \tag{11}$$

where a_i, b_i, c_i, d_i, e_i, f_i, and g_i are constant coefficients that were determined by performing a least square method (Sauer 2014). The optimum values of these constant coefficients are shown in Table 2.

The value of R^2 of the proposed new stability criterion is about 99.98%, meaning that the approximation from Eq. (6) fits the FELA results very well. Figure 9 shows that N_γ is a function of C/D only and the relationship between the two is linear. Note that N_γ is negative for $C/D<2.5$. This means that for cavities at relatively small depths, the self-weight of the ground has a positive effect on the limit load (i.e., σ_s increases with γ). Intuitively, this is not right.

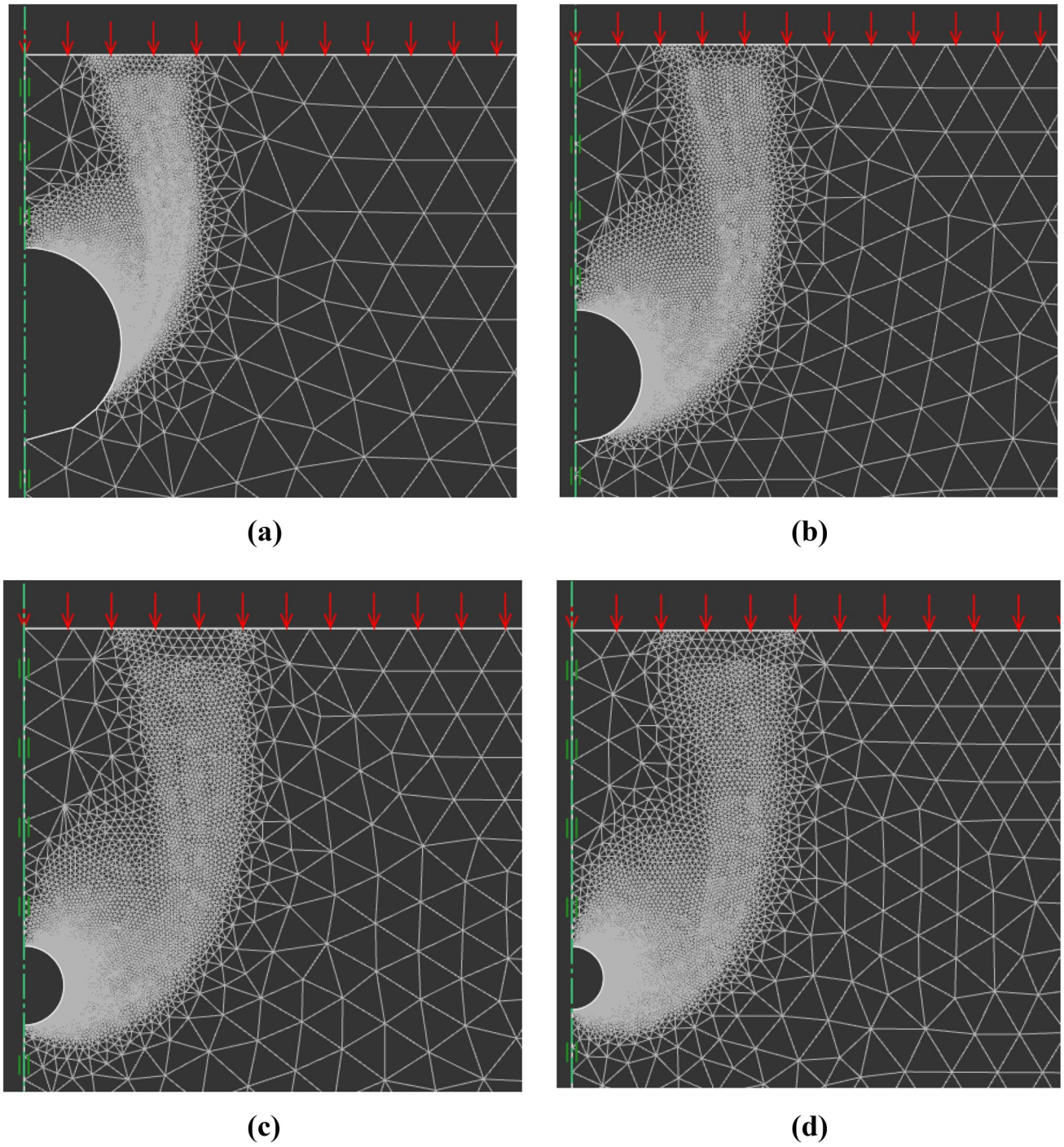

Fig. 7 Upper bound axisymmetric mesh for various cover depth ratios *C/D* (GSI = 80, $m_i = 10$, $\sigma_{ci}/\gamma D = 100$) **a** *C/D* = 1, **b** *C/D* = 2, **c** *C/D* = 4 and **d** *C/D* = 5

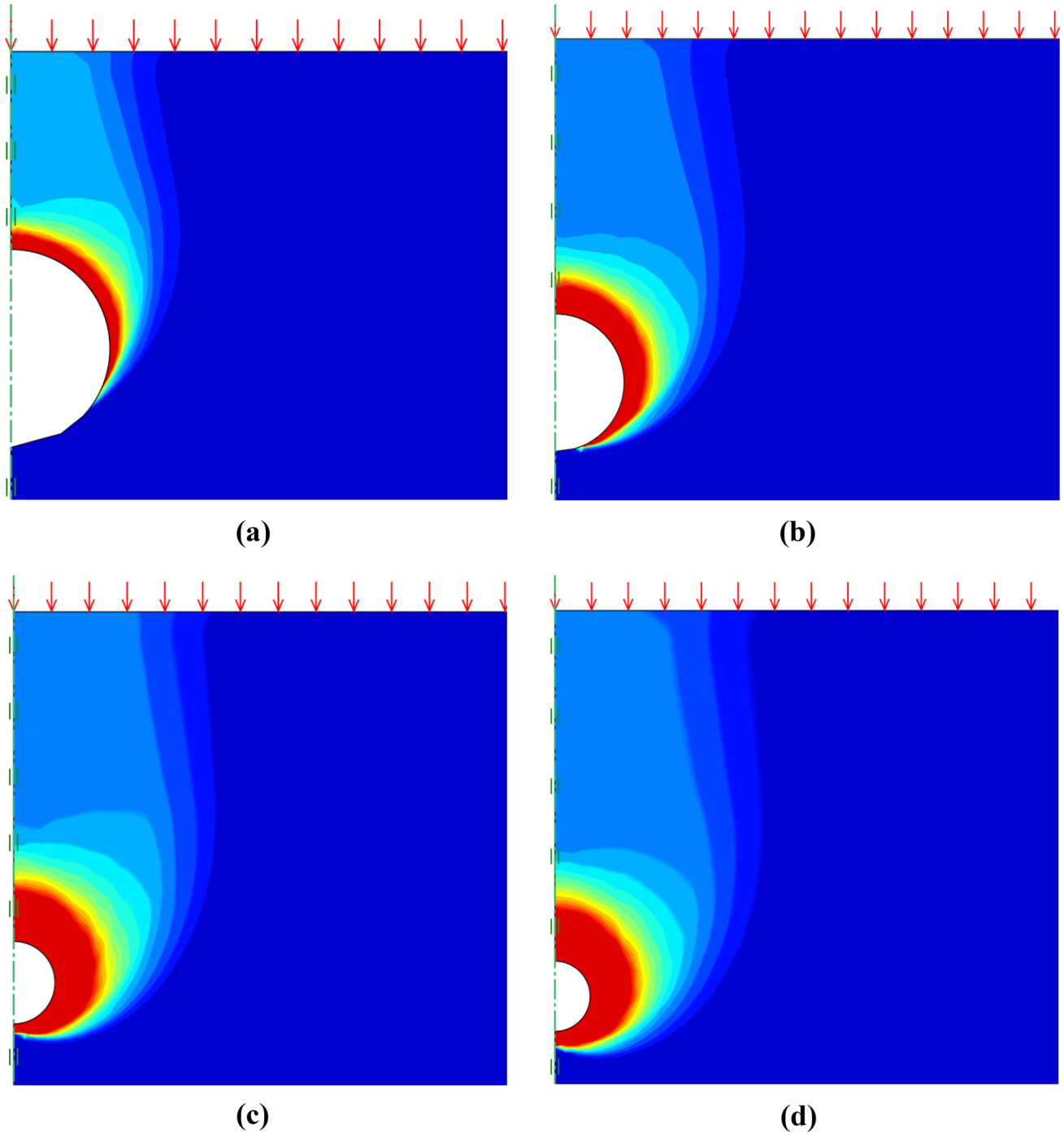

Fig. 8 Shear power dissipation contours for various cover depth ratios C/D ($GSI = 80$, $m_i = 10$, $\sigma_{ci}/\gamma D = 100$) **a** $C/D = 1$, **b** $C/D = 2$, **c** $C/D = 4$ and **d** $C/D = 5$

Table 2 Constants for the design equation

a_1	a_2	b_1	b_2
8.8310	−3.5150	9.7852×10^{-2}	−0.1116
b_3	c_1	c_2	c_3
1.7318×10^{-2}	-1.1060×10^{-3}	1.4627×10^{-3}	-2.1621×10^{-4}
d_1	e_1	e_2	f_1
3.9885×10^{-6}	0.3070	−0.4847	-1.5624×10^{-2}
f_2	f_3	g_1	g_2
3.5499×10^{-2}	-6.8341×10^{-4}	1.2109×10^{-4}	-5.4357×10^{-4}

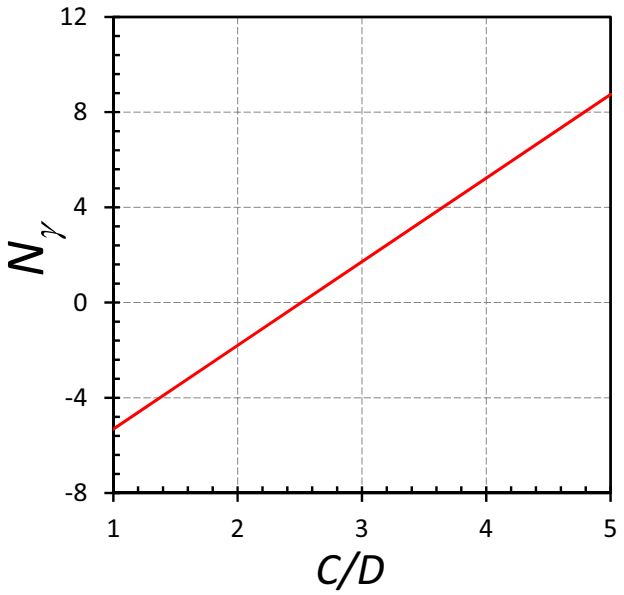

Fig. 9 The factor $N\gamma$

Nevertheless, by taking another look at Eqs. (7, 9, and 10) would have explained this. Noting that the values of (F_1, F_2, and N_c) become small when $C/D < 2.5$, it may result in a total decrease of σ_s (see Eq. 6). On the other note, Fig. 10 shows that N_c is a function of both C/D and GSI for the given values of $m_i = 5$, 10, 20, and 30. In general, N_c increases nonlinearly as the cover depth C/D increases for all GSI values selected in the figures. The rate of increase is different for each GSI value. The curve becomes flattered (gradient decrease) as GSI decreases.

5 Conclusions

This short technical note has successfully studied the stability of spherical cavity in axisymmetric Hoek–Brown rock mass using the rigorous upper and lower bound finite element limit analysis. The solution was formulated to find the limit normalized surface pressures σ_s/σ_{ci} that is a function of four dimensionless parameters; namely the cover-depth ratio C/D, the Geological Strength Index GSI, the Hoek–Brown m_i parameter, and the normalized uniaxial compressive strength $\sigma_{ci}/\gamma D$. A new stability criterion for predicting the stability of cavities in rock masses is developed by using a least square method of the computed solutions. The main findings of the present study are summarized as follows.

- The limit normalized surface pressures σ_s/σ_{ci} increases as the cover depth ratio C/D increases. The greater the values of GSI and m_i, the larger the $\sigma_s/\sigma_{ci.}$ In addition, the effect of $\sigma_{ci}/\gamma D$ on σ_s/σ_{ci} is insignificant for all considered depth ratios in this study.
- The failure mechanism of a cavity resembles a chimney type of vertical slippage when C/D is small. The lateral size of the failure mechanism extends when C/D increases.
- The new cavity stability factors N_c and N_γ for the stability of cavities in rock masses are proposed in this paper, where N_c is a function of C/D only while N_γ is a function of C/D, GSI, and m_i.

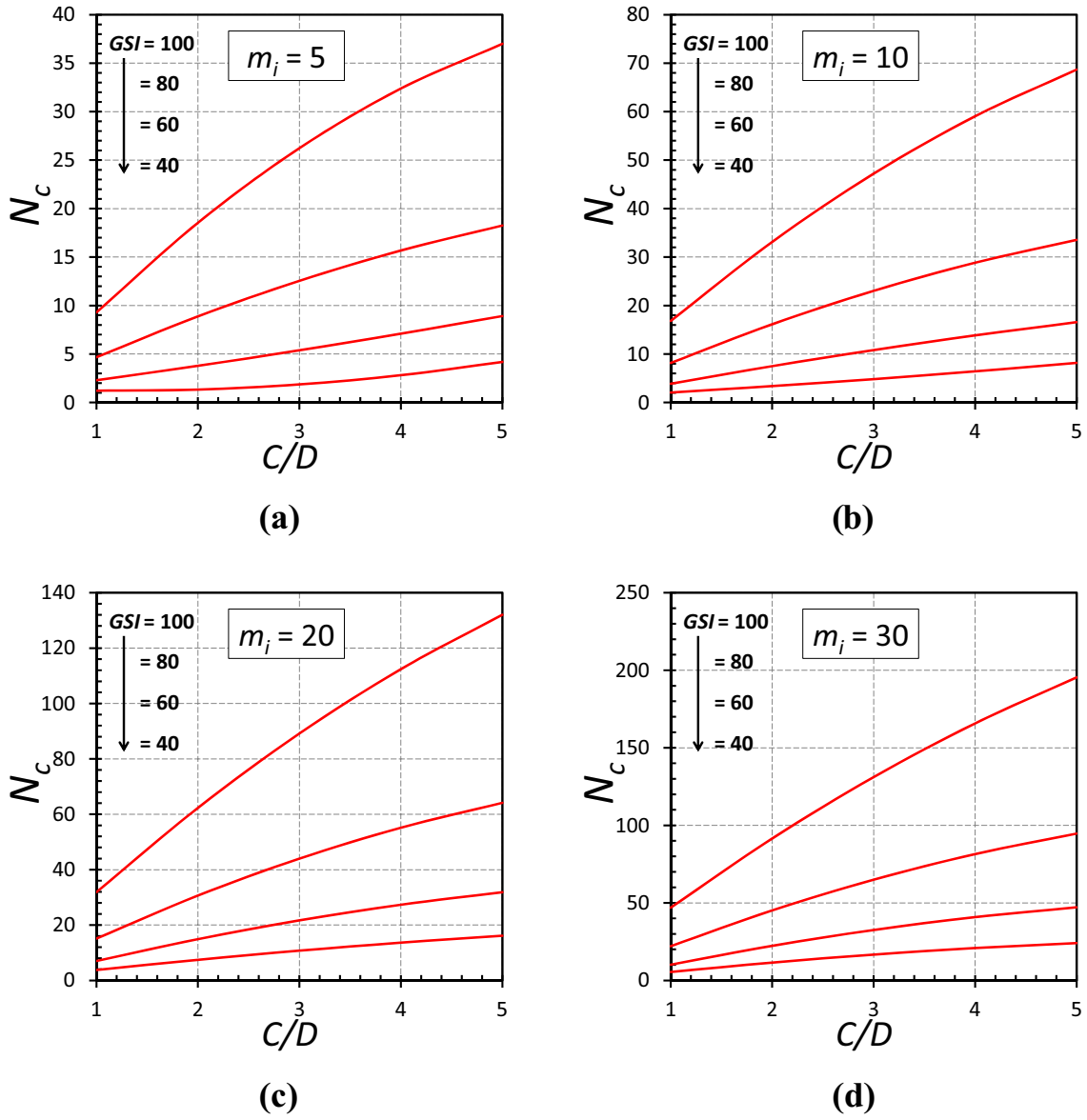

Fig. 10 The factor N_c **a** $m_i = 5$; **b** $m_i = 10$; **c** $m_i = 20$; and **d** $m_i = 30$

Funding Open Access funding enabled and organized by CAUL and its Member Institutions.

References

Abdulla WA, Goodings DJ (1996) Modelling of sinkholes in weakly cemented sand. J Geotech Eng 122–12:998–1005

Abdulla WA (1995) Centrifuge modelling of sinkhole development in weakly cemented sand [PhD dissertation]. University of Maryland

Augarde CE, Lyamin AV, Sloan SW (2003) Prediction of undrained sinkhole collapse. J Geotech Geoenviron Eng 129:197–205

Ciria H, Peraire J, Bonet J (2008) Mesh adaptive computation of upper and lower bounds in limit analysis. Int J Numer Meth Eng 75:899–944

Craig WH (1990) Collapse of cohesive overburden following removal of support. Can Geotech J 27:355–364

Drucker DC, Prager W, Greenberg HJ (1952) Extended limit design theorems for continuous media. Q Appl Math 9:381–389

Drumm EC, Kane WF, Yoon CJ (1990) Application of limit plasticity to the stability of sinkholes. Eng Geol 29:213–225

Fraldi M, Guarracino F (2009) Limit analysis of collapse mechanisms in cavities and tunnels according to the Hoek-Brown failure criterion. Int J Rock Mech Min Sci 46:665–673

Hoek E, Carranza-Torres C, Corkum B (2002) Hoek–Brown failure criterion—2002 edition. In: Proceedings of the North American rock mechanics society meeting in Toronto

Huang F, Zhao L, Ling T, Yang X (2017) Rock mass collapse mechanism of concealed karst cave beneath deep tunnel. Int J Rock Mech Min Sci 91:133–138

Keawsawasvong S (2021) Limit analysis solutions for spherical cavities in sandy soils under overloading. Innov Infrastruct Solut 6:33

Keawsawasvong S, Ukritchon B (2019) Undrained stability of a spherical cavity in cohesive soils using finite element limit analysis. J Rock Mech Geotech Eng 11:1274–1285

Keawsawasvong S, Ukritchon B (2020) Design equation for stability of shallow unlined circular tunnels in Hoek-Brown rock masses. Bull Eng Geol Env 79(8):4167–4190

OptumCE (2019) OptumG2. Copenhagen, Denmark: Optum Computational Engineering. See https://optumce.com/

Rahaman O, Kumar J (2020) Stability analysis of twin horse-shoe shaped tunnels in rock mass. Tunn Undergr Space Technol 98:103354

Sauer T (2014) Numerical analysis. Pearson Education Limited, London, UK

Shiau J, Al-Asadi F (2020) Three-dimensional analysis of circular tunnel headings using Broms and Bennermarks' Original Stability Number. Int J Geomech 20(7):0001734

Shiau J, Lamb B, Sams M (2016a) The use of sinkhole models in advanced geotechnical engineering teaching. Int J Geomate 10(2):1718–1724

Shiau J, Sams M, Lamb B (2016b) Introducing advanced topics in geotechnical engineering teaching–tunnel modelling. Int J Geomate 10(1):1698–1705

Shiau J, Lee JS, Al-Asadi F (2021) Three-dimensional stability analysis of active and passive trapdoors. Tunn Undergr Space Technol 107:103635

Shiau J, Smith C (2006) Numerical analysis of passive earth pressures with interfaces. In Proceedings of the III European Conference on Computational Mechanics (ECCM 2006), 5–8 June 2006, Lisbon, Portugal

Sloan SW (2013) Geotechnical stability analysis. Géotechnique 63(7):531–572

Tharp TM (1999) Mechanics of upward propagation of cover collapse sinkholes. Eng Geol 52:23–33

Ukritchon B, Keawsawasvong S (2019a) Stability of unlined square tunnels in Hoek-Brown rock masses based on lower bound analysis. Comput Geotech 105:249–264

Ukritchon B, Keawsawasvong S (2019b) Lower bound stability analysis of plane strain headings in Hoek-Brown rock masses. Tunn Undergr Space Technol 84:99–112

Vaziri HH, Jalali JS, Islam R (2001) An analytical model for stability analysis of rock layers over a circular opening. Int J Solids Struct 38:3735–3757

Wu G, Zhao M, Zhang R, Liang G (2020) Ultimate bearing capacity of eccentrically loaded strip footings above voids in rock masses. Comput Geotech 128:103819

Xiao Y, Zhao M, Zhao H, Zhang R (2018) Finite element limit analysis of the bearing capacity of strip footing on a rock mass with voids. Int J Geomech 18(9):04018108

Xiao Y, Zhao M, Zhang R, Zhao H, Wu G (2019) Stability of dual square tunnels in rock masses subjected to surcharge loading. Tunn Undergr Space Technol 92:103037

Xiao Y, Zhang R, Zhao M, Jiang J (2021) Stability of unlined rectangular tunnels in rock masses subjected to surcharge loading. Int J Geomech 21(1):04020233

Zhang R, Xiao Y, Zhao M, Zhao H (2019) Stability of dual circular tunnels in a rock mass subjected to surcharge loading. Comput Geotech 108:257–268